

Machine Learning Based NLOS Radio Positioning in Beamforming Networks

Roman Klus*, Jukka Talvitie*, Julia Vinogradova[†], Johan Torsner[†], and Mikko Valkama*

*Faculty of Information Technology and Communication Sciences, Tampere University, Tampere, Finland

[†]Ericsson Research, Helsinki, Finland

Abstract—In this paper, we address the challenging problem of radio positioning in non-line-of-sight (NLoS) conditions. To this end, we utilize measurements in the form of time-of-flight and gNodeB angular information in the context of 5G New Radio (NR) networks. Such measurements are processed by artificial neural networks with different snapshot and sequence-processing architectures to track the positions of the terminals. For model training, we consider a crowdsensing data acquisition scheme to effortlessly gather the desired measurements with the synchronized location tags. Realistic ray-tracing based evaluations on the so-called Madrid map at 28 GHz millimeter-wave band are provided, to assess the achievable performance while also varying the amount of uncertainties within the data. The obtained results show that radio positioning is feasible with accuracy in the order of 1 meter, or even below, also in challenging NLoS scenarios if the data and measurement uncertainties are small. The results also show that the sequence processing approach offers superior performance under practical measurement uncertainties.

Index Terms—5G, beamforming, crowdsensing, deep learning, LSTM, neural networks, NLoS, positioning

I. INTRODUCTION

To enhance the network capacity, throughput and latency characteristics, the Fifth Generation (5G) New Radio (NR) standard supports operation at the so-called Frequency Range 2 (FR2) that refers to the millimeter-wave (mmWave) bands between 24.25 and 52.6 GHz [1]. On one hand, higher frequencies offer higher data rates, extremely low latency, and enable new ways to achieve efficient spatial diversity by applying beamforming schemes. On the other hand, due to stronger signal attenuation by the environment, densified base station (BS) deployments are also required, especially in densely built areas, where Line-of-Sight (LoS) between the User Equipment (UE) and BS is challenging to ensure at all times. To this end, real-time and highly accurate UE location tracking becomes necessary for numerous Location-Based Services (LBS), while also supporting the network resource allocation, mobility management and beam management. While in the open areas the Global Navigation Satellite System (GNSS) positioning is reliable and accurate, tall buildings blocking the satellite signals raise the demand for alternative positioning schemes in urban, industrial and indoor areas.

In general, non-GNSS positioning is based on utilizing signals of opportunity, e.g. reference signals in 5G networks, and a suitable algorithm that is able to estimate the UE position based on prior knowledge in the area and the incoming signal measurements. In most of the existing works, localization is based on proximity, Reference Signal Received Power (RSRP)

measurements, Channel State Information (CSI), time measurements, angle measurements, or their combinations [2], [3], whereas the matching algorithm can be a probabilistic model, Neural Network (NN) [4], k -Nearest Neighbors (k -NN) [5] or Path-Loss (PL) model, among others [6]. Furthermore, simultaneous mobility management and localization were addressed and evaluated in [7], achieving meter-level accuracy as the by-product of the mobility management model.

The implementation of artificial intelligence into the mobile networks is, in general, one of the key transformations between 5G and 6G [8], where the training and operation of the Machine Learning (ML) models are clearly defined. To this end, in this work, we investigate the 5G FR2 network capabilities for UE positioning in realistic urban deployment, under limited availability of the LoS. We develop a ML model capable of extracting useful information and finding accurate user position even in Non-Line-of-Sight (NLoS), while working in compliance with latest 3rd Generation Partnership Project (3GPP) standards. Additionally, we propose a dataset acquisition scheme without performing a dedicated site-survey, consequently cutting the network deployment costs.

The 5G network's current capabilities to perform positioning task are described in [9], including the network measurements considered in this work. Similar to our work, [10] targets the 5G FR2 positioning in the urban deployment, while considering beam-RSRP measurements as the features for the NN positioning model. The authors properly define their positioning model's co-existence within the current networks, but consider only perfect ray-tracing data with no uncertainties, discard all measurements that do not include LoS, and utilize only a simple NN model.

Compared to the existing literature, the main contributions of this work are as follows:

- 1) We propose a standard-compliant crowdsensing scheme for constructing measurement databases, capable of including channel state, power, angular measurements, as well as the timed reference location tags.
- 2) We propose a regularized sequence-processing NN model for positioning in urban scenarios, capable of mitigating uncertainties from network signal measurements, as well as from the reported locations included within the training data.
- 3) We evaluate the capability of the considered models with realistic ray-tracing data and show their positioning capabilities in varying scenarios and under different

uncertainty values, demonstrating that the reported inaccuracies within the crowdsensed data are strongly diminished when using the sequence-processing solution.

The rest of this paper is organized as follows: Section II describes the system model and data acquisition scheme. Section III presents the utilized ML models. Section IV describes the evaluation environment and the numerical results. Finally, Section V concludes this work.

II. SYSTEM MODEL AND MEASUREMENTS

In this section we present a standard-compliant crowdsensing scheme, which enables training database acquisition without costly and time-consuming measurement campaigns. The training database includes the Time-of-Flight (ToF), angular information in terms of either Angle-of-Departure (AoD) or Angle-of-Arrival (AoA) at the BS called gNodeB, and the synchronized location tag for each sample.

A. Training Data Acquisition in NR

The location information exchange can be implemented using Minimization of Drive Testing (MDT) approach, first introduced in 3GPP Release 10 and currently specified in 3GPP specification #37.320 for Rel. 16. The idea behind MDTs is setting the UE to either log or periodically send the reports about the network measurements, including the current UE location and timestamps. In NR networks, the reported quantities include RSRP, best beam index, indexes of beams with RSRPs above the pre-defined threshold, and therefore enabling the smooth and timed location information transfer to the gNodeB. We assume that coarse location information can be obtained in the training phase using GNSS, while taking into account the large uncertainties of such reference data in practical urban environments in our numerical experiments.

The ToF measurement is, in general, not directly included in the NR networks, but is possible to obtain from the other measurements and reports. Specifically, the ToF can be acquired, e.g., from the Multi-Round Trip Time (MRTT) measurements [11]. The ToF at the BS can be obtained from the reported "UE Rx-Tx time difference" Physical Layer (PHY) measurement from the UE, as specified in [12]. The measurement specifies the time difference between receiving the first detected path in time of the specific downlink subframe and transmitting a specific uplink subframe, closest in time to the received one. The timing of the measured subframes is known at the BS. Assuming the negligible timing and propagation delays compared to the UE velocity, the ToF is then obtained as:

$$ToF = \{t_{RX}^{BS} - t_{TX}^{BS} - T_{TX-RX}^{UE}\}/2 \quad (1)$$

where t_{RX}^{BS} is the timestamp of BS transmitting the downlink (DL) subframe, t_{TX}^{BS} is the timestamp of BS receiving the uplink (UL) subframe, and T_{TX-RX}^{UE} refers to the reported UE Rx-Tx time difference, considering two aforementioned subframes. Furthermore, the angular information at the BS can be obtained either from the UL-AoA measurements or by assuming the correct beam configuration for DL transmission.

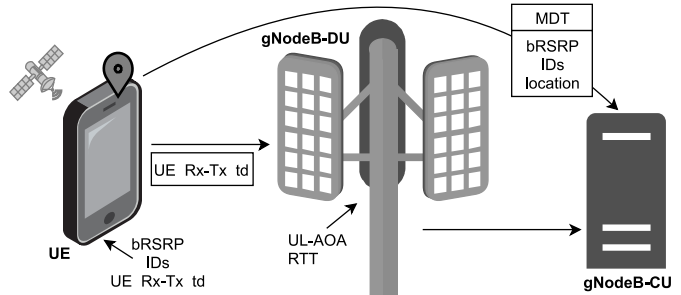


Fig. 1. Data acquisition work-flow within the NR network.

The complete database acquisition scheme is illustrated in Fig. 1.

We also note that alternatively, the ToF can be obtained indirectly at the gNodeB via Time-Difference-of-Arrival (TDoA) and the related positioning calculations, as defined in [11]. Furthermore, extended Kalman filter (EKF) based approaches to estimate and track the AoA and ToF from the uplink signals have also been described in [13]. However, the presented solutions assume, in general, the availability of LoS.

B. Data Flow and Operational Alternatives

As described above, the angular information is directly available at the gNodeB Decentralized Unit (DU), while the ToF information can be acquired from Multi-Round Trip Time (RTT) and the reported measurements. Thus, the positioning using the considered measurements at the gNodeB side is directly feasible. In principle, however, the same procedure can be implemented at the UE, with the downlink AoD information and the Multi-RTT reported to the UE from the positioning server [11]. In such cases, additional measures are needed to provide the UE with the trained ML model. In this paper, in the continuation, we focus on the network side positioning for presentation simplicity.

III. ML METHODS

A. ML Models

In this work, we consider three distinct models to evaluate the capability of the system to perform the positioning task. First, as the benchmark model, we consider a k -NN model with the Manhattan distance as the matching metric and the number of considered neighbors k equal to 7, which was found to be optimal by sweeping over different values of k and minimizing the positioning error. The k -NN algorithm does not perform actual model training, but the prediction phase is costly, as it manually searches for the most similar samples across the whole training database.

The second considered model, further denoted as Dense Neural Network (DNN), is a snapshot NN with two densely connected hidden layers, followed by a dropout regularization. The architecture is depicted in Fig. 2 (top), along with the chosen hyperparameters. The model was trained on 38 tracks dedicated for training for up to 200 epochs in total, with mean squared error as the loss function, Adam regularizer and

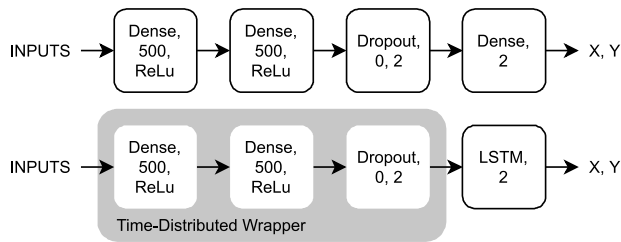


Fig. 2. The architectures of the DNN (top) and Long-Short Term Memory (LSTM) (bottom) models. The last layer of each model has linear (identity) activation function. The model inputs (snapshots for DNN and sequences for LSTM) are as described in Section III-B, and the outputs are the UE coordinates.

the decreasing learning rates from 0.001, until convergence. The two-hidden layer architectures were found sufficient by parameter sweeping, as well as by the recommendation in the literature [10].

The third model takes into consideration also the temporal dependencies within the data. Its architecture is similar to that of the DNN model, apart from the fact that the intermediate layers are wrapped in the time-distributed layer, and its output is a LSTM layer with two units. The time-distributed wrapper allows densely connected layers to co-exist within the same model as the sequence-processing layers. The LSTM model’s architecture is depicted in Fig. 2 (bottom). It considers sequences with maximum length of 10 samples, estimates only the coordinates of the last sample, and was trained with the same hyperparameters as the DNN model for fair performance comparison.

B. Data Characteristics and Uncertainties

The data considered by the proposed models to acquire the user location include ToF, and the BS angular information, as either DL AoD or UL AoA. Their practical acquisition follows the schemes described in Section II. To ensure the consistency of the features, the ToF is casted into the pseudo-range through the speed of light. The considered signal paths, that include pseudo-range, azimuth and elevation angles, are then transformed from spherical into the Cartesian coordinates. After normalization, the resulting x , y , and z distances are then used as the model inputs.

As the considered data acquisition scheme builds on the crowdsensed location estimates through GNSS, perfect label accuracy cannot be assumed. Thus, in the numerical evaluations, we add additive white Gaussian noise (AWGN) of different powers or standard deviation σ_{xy} to the location labels. An example with $\sigma_{xy} = 10$ m is shown in Fig. 3 as the blue track. Similarly, in order to model the network measurement uncertainties and imperfections, we add the AWGN uncertainty to the measured pseudo-ranges, parameterized with σ_r , as well as deliberately limit or quantize the angle measurements to consider the effects of implementation feasible fixed-beam antenna arrays at mmWaves.

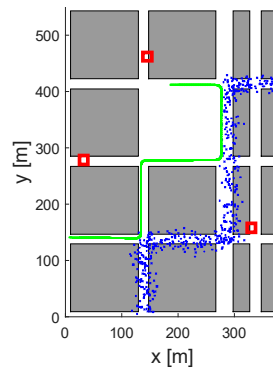


Fig. 3. Deployment scenario with highlighted BS locations (red), and two example paths, one with no uncertainties in the labels (green), the other skewed with normally distributed uncertainty with $\sigma_{xy} = 10$ m (blue).

IV. NUMERICAL RESULTS AND ANALYSIS

A. Evaluation Environment

We utilize ray-tracing-based channel measurements based on Wireless Insite@software [14] in the Madrid grid proposed by the METIS society [15], recognized also by 3GPP in 5G NR specifications [16]. The Madrid grid layout introduces a rich radio propagation environment with different street widths and open areas, as illustrated in Fig. 3.

The simulated area includes 3 BSs, each equipped with a uniformly-spaced cylindrical antenna array containing 4 elevated layers with 16 antenna elements per layer. The simulations are performed in DL using a 28 GHz carrier frequency. The AoD and ToF measurements are obtained based on the corresponding characteristics of the radio propagation path with the highest received power. The effective PL threshold for considering any particular BS link per measurement instance is set to -160 dB.

The dataset consists of 40 separate vehicle-like user tracks, as shown in Fig. 3, where UE collects measurements at 100 ms intervals. The UE locations are initialized with random locations and the UE moves in the area by considering an equal probability to advance in any direction from intersections. The UE velocity varies between 20 and 60 km/h depending on the present street and possible proximity of intersections. When approaching an intersection, the UE decelerates. After the turn, the UE accelerates until reaching a street-specific speed limit. Although all user tracks follow the right-hand traffic characteristics, the exact UE trajectories are different for each simulated user track. The dataset consists of 25181 samples.

For implementing and training ML models, the majority of this work was realized in Python 3.6 programming environment, while utilizing the following libraries: TensorFlow, SciPy, NumPy, Pandas and scikit-learn. The final evaluation and visualization of the results were realized in MATLAB R2020b.

B. Results

In this section, we evaluate the performance of the considered crowdsensing scheme and the ML positioning models in

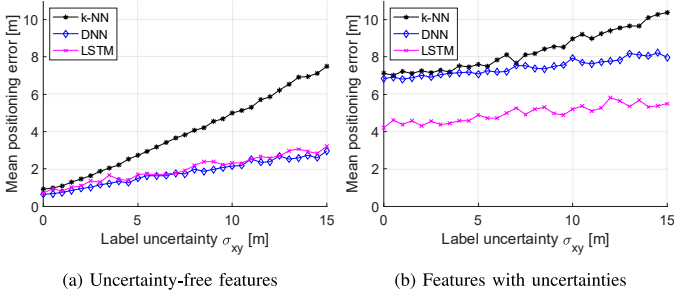


Fig. 4. MEE of different models. In (a), perfect pseudo-range and angle measurements are considered, while in (b) the pseudo-range is subject to random Gaussian uncertainty of $\sigma_r = 10$ m and the angle measurements are quantized to 20° resolution.

the Madrid grid deployment. The considered data, including ToF, AoA, and the positioning labels were contaminated using additive uncertainties and imperfections to imitate the real-world obstructions within the data. From the 40 user paths through the environment, 38 were chosen for training the model and the remaining 2 were used for evaluation.

The models' susceptibility to the uncertainties within the training labels are first depicted in Fig. 4a, in terms of the positioning Mean Euclidean Error (MEE). We can clearly observe that the positioning performance depends on the accuracy of the training labels, parametrized with σ_{xy} . The figure shows the sub-meter accuracy of the k -NN, DNN and LSTM models when working on uncertainty-free data, yet with increasing uncertainty the k -NN's performance decreases substantially faster than those of the NN models. The LSTM model, despite considering also previous samples, has almost no effect on the performance.

Fig. 4b shows and compares then the positioning performance with the practical uncertainties added also to the ranging and angular measurements. Specifically, $\sigma_r = 10$ m is considered to reflect fairly large uncertainties in the pseudo-range estimates, stemming in practice for example from clock offsets and drifting, while the angular resolution is coarsely limited and quantized to 20° in both elevation and azimuth domains. The corresponding results in Fig. 4b show the improved performance of the LSTM model over the other two approaches. Thus, when working under large uncertainties in the data, the sequence approach utilizing the temporal correlation provides clear performance benefits.

Furthermore, we compare the error distributions of the three models in three distinct uncertainty scenarios, presented in Fig. 5. First, we visualize the positioning accuracy in uncertainty-free scenario, where the DNN model achieves the lowest errors with 0.64 m mean and 0.40 m median positioning error. The k -NN's mean and median performance are slightly poorer, namely 0.93 m and 0.43 m, while the LSTM achieves 0.69 m and 0.48 m mean and median positioning errors, respectively. The second set of boxplots refers to the case with uncertainty-free features and imperfect labels ($\sigma_{xy} = 10$ m). Here, both NN models outperform the k -NN, DNN achieving 2.2 m and LSTM achieving 2.3 m mean positioning error. The

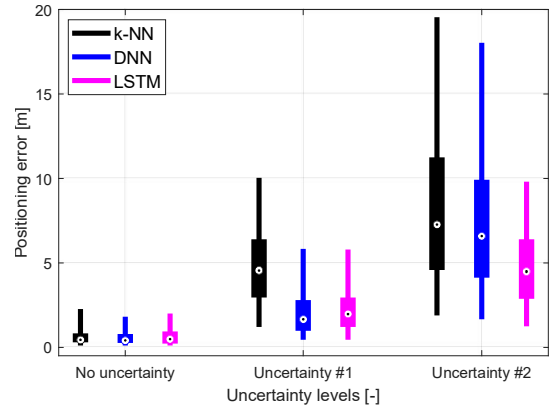


Fig. 5. Comparison of positioning error distributions for different uncertainty scenarios. Uncertainty #1 (middle) refers to $\sigma_{xy} = 10$ m, $\angle^\circ = 0^\circ$, and $\sigma_r = 0$ m. Uncertainty #2 (right) refers to $\sigma_{xy} = 10$ m, $\angle^\circ = 20^\circ$, and $\sigma_r = 10$ m. The point in the middle denotes median, boxes range from 25^{th} to 75^{th} percentiles, and whiskers mark 5^{th} and 95^{th} percentiles of the positioning error distributions.

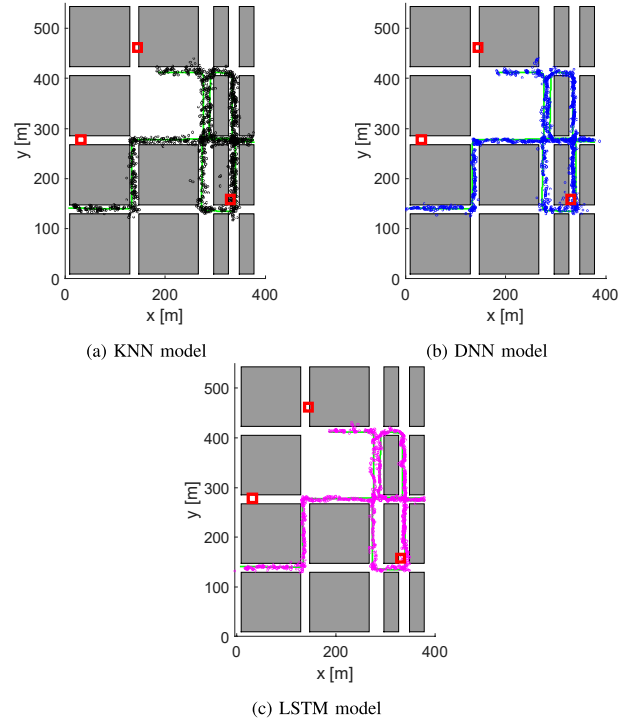


Fig. 6. Visual illustration of the true (green) and estimated UE location traces in high-uncertainty scenario with $\sigma_{xy} = 10$ m, $\angle^\circ = 20^\circ$, and $\sigma_r = 10$ m.

last set of boxplots refers to the scenario with $\sigma_{xy} = 10$ m, angle resolution $\angle^\circ = 20^\circ$, and ranging uncertainty $\sigma_r = 10$ m. Here, the LSTM model outperforms the other two, DNN achieving more than 60% higher mean positioning error, and k -NN resulting in 89% higher MEE than the LSTM model with 4.9 m of MEE. The outliers are also reduced significantly, visualized as whiskers of the boxes.

An additional visual illustration of the different models and their capabilities are depicted in Fig. 6, which shows the test path estimations in high-uncertainty scenario ($\sigma_{xy} = 10$ m,

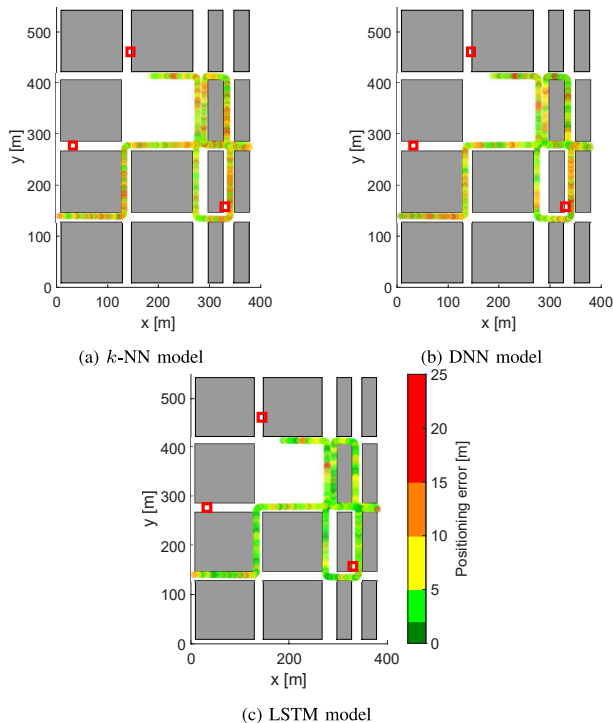


Fig. 7. Positioning error heat maps for the different considered models under large uncertainties of $\sigma_{xy} = 10$ m, $\angle^\circ = 20^\circ$, and $\sigma_r = 10$ m.

$\angle^\circ = 20^\circ$, and $\sigma_r = 10$ m). The location estimates are plotted on top of the true coordinates, which are shown as green lines. Fig. 6 also displays the locations of the BSs as red squares. The plotted results show the high variance of the k -NN model's estimates in Fig. 6a, already significantly lower dispersion of the estimates of the DNN model in Fig. 6b, and finally the highly stable paths in Fig. 6c representing the LSTM model's location estimates.

Similar comparison is shown in Fig. 7, where the positioning errors are represented using a heat map. The scale of the colorbar is limited to 25 m to better visualize the continuous trends in the estimated locations. The results of different models in Fig. 7a for k -NN, Fig. 7b for DNN, and Fig. 7c for LSTM, clearly show that the LoS link between the UE and the BS does not necessarily guarantee beneficial conditions for accurate positioning. According to the results in Fig. 6 and Fig. 7, the highest positioning errors occur directly beneath the base stations (see bottom-right corner), in the poorly covered areas (bottom-left street), and in the cross-sections between the LoS and NLoS.

V. CONCLUSION

In this paper, we considered, formulated and evaluated three different models, namely k -NN, snapshot NN and sequence-processing LSTM models, for radio positioning in urban deployments of beamforming-based 5G mmWave networks with emphasis on NLoS scenarios. We described a data acquisition scheme capable of collecting synchronized user and network-centric data, and combining them into an efficient positioning database. For realistic performance evaluations and

assessment, also practical uncertainties in the training locations as well as in the assumed ToF and angular measurements were considered. The reported ray-tracing based numerical results at 28 GHz show that all three models perform similarly in the uncertainty-free reference scenario, achieving sub-meter mean positioning errors. Furthermore, accounting for uncertainty within the location labels results in the two NN models outperforming the k -NN, yet the additional temporal information in LSTM provides no additional benefit. Finally, the LSTM outperforms the snapshot-based models by a large margin in the practical case when the uncertainties are also included in the ToF and angle measurements, serving as the considered features. Our future work will focus on extending the work to consider also beam-RSRP measurements as well as beam-based complex channel impulse responses as the neural network features.

ACKNOWLEDGMENT

The work was supported in part by Ericsson and in part by the Academy of Finland under the grants #328214 and #323244.

REFERENCES

- [1] E. Dahlman *et al.*, *5G NR: The Next Generation Wireless Access Technology*, 2nd ed. Elsevier, 2020.
- [2] S. Subedi *et al.*, "A survey of smartphone-based indoor positioning system using RF-based wireless technologies," *Sensors*, vol. 20, no. 24, p. 7230, 2020.
- [3] C. Laoudias *et al.*, "A survey of enabling technologies for network localization, tracking, and navigation," *IEEE Commun. Surveys Tuts.*, vol. 20, no. 4, pp. 3607–3644, 2018.
- [4] R. Klus *et al.*, "Transfer learning for convolutional indoor positioning systems," in *2021 Int. Conf. on Indoor Positioning and Indoor Navigation (IPIN)*. IEEE, 2022, pp. 1–8.
- [5] L. Klus *et al.*, "RSS fingerprinting dataset size reduction using feature-wise adaptive k-means clustering," in *2020 12th Int. Congress on Ultra Modern Telecommunications and Control Systems and Workshops (ICUMT)*. IEEE, 2020, pp. 195–200.
- [6] F. Zafari, A. Gkelias, and K. K. Leung, "A survey of indoor localization systems and technologies," *IEEE Commun. Surveys Tuts.*, vol. 21, no. 3, pp. 2568–2599, 2019.
- [7] R. Klus *et al.*, "Deep learning based localization and HO optimization in 5G NR networks," in *2020 Int. Conf. on Localization and GNSS (ICL-GNSS)*. IEEE, 2020, pp. 1–6.
- [8] K. B. Letaief *et al.*, "The roadmap to 6G: AI empowered wireless networks," *IEEE communications magazine*, vol. 57, no. 8, pp. 84–90, 2019.
- [9] S. Dwivedi *et al.*, "Positioning in 5G networks," *IEEE Communications Magazine*, vol. 59, no. 11, pp. 38–44, 2021.
- [10] M. M. Butt *et al.*, "ML-assisted UE positioning: Performance analysis and 5G architecture enhancements," *IEEE Open Journal of Vehicular Technology*, vol. 2, pp. 377–388, 2021.
- [11] 3GPP, "Stage 2 functional specification of User Equipment (UE) positioning in NG-RAN," Tech. Rep. 38.305, 12 2021, version 16.7.0.
- [12] 3GPP, "Physical layer measurements," Tech. Rep. 38.215, 1 2021, version 16.4.0.
- [13] M. Koivisto *et al.*, "Joint device positioning and clock synchronization in 5G ultra-dense networks," *IEEE Transactions on Wireless Communications*, vol. 16, no. 5, pp. 2866–2881, 2017.
- [14] Remcom. Wireless InSite - 3D wireless prediction software. Accessed: Jan 27, 2021. [Online]. Available: <https://www.remcom.com/wireless-insite-em-propagation-software>
- [15] A. Rauch *et al.*, "Fast algorithm for radio propagation modeling in realistic 3-D urban environment," *Advances in Radio Science*, vol. 13, pp. 169–173, 11 2015.
- [16] 3GPP, "Study on channel model for frequencies from 0.5 to 100 GHz positioning in NG-RAN," Tech. Rep. 38.901, 12 2019, version 16.1.0.